Full-Wave Analysis of Multiconductor Multislot Planar Guiding Structures in Layered Media

Ezzeldin A. Soliman, *Associate Member, IEEE*, Guy A. E. Vandenbosch, *Member, IEEE*, Eric Beyne, and Robert P. Mertens, *Fellow, IEEE*

***Abstract*—In this paper, a generalized two-dimensional formulation for solving planar guiding structures is presented. The formulation is capable of analyzing guiding structures consisting of an arbitrary number of slots and strips with arbitrary width, thickness, and conductivity in a full-wave regime. Integral equations solved with the method of moments in the spatial domain are used in the analysis. All information related to the fundamental modes of the guiding structure are available from the presented theory. These information include (for each mode) the propagation constant, electric and magnetic current distribution, modal power, and the characteristic impedance. Numerical results for a number of planar guiding structures are presented, which validate the proposed theoretical formulation.**

***Index Terms*—Integral equation formulation, method of moments (MoM), planar guiding structures.**

I. Introduction

ADVANCES IN packaging and integrated circuit technology force the lines used as interconnects between the systems' components to be very close to each other. As a consequence, the mutual coupling between these lines is no longer negligible. This necessitates treating them as a single guiding structure capable of supporting several modes, rather than several isolated transmission lines. Also, the intensive amount of data transmission in high-speed digital communications requires studying the dispersion characteristics of the fundamental modes of a planar guiding structure very carefully for a precise design. These technological and design considerations explain the interest given by several authors in the past two decades toward planar guiding structures. Several numerical techniques have been applied to planar guiding structure problems. These techniques can be classified into two main categories: 1) the quasi-TEM, or quasi-static, approach and 2) the full-wave approach.

The quasi-static approach simplifies the formulation. It can be considered as a low-frequency approximation which neglects the longitudinal electric and magnetic fields supported by the guiding structure [1], [2]. These longitudinal field components result in the well-known physical dispersion phenomenon. As the operating frequency increases, the dispersion characteristics of the guiding modes become of practical importance for a precise design for communication systems. These requirements automatically lead to the full-wave approach.

The full-wave approach can be further categorized into: 1) the differential equation formulation and 2) the integral equation formulation. In the differential equation formulation, the unknowns to be solved for are the electromagnetic fields in a computation volume [3], [4]. As one would expect, this formulation is quite memory and computation time consuming. The second category within the full-wave approach is the integral equation formulation. This formulation solves for the unknown electric and magnetic currents on electric conductors and slots, respectively. After obtaining the unknown electric and magnetic current, the electromagnetic field becomes available in the domain of interest. Obviously, the integral equation formulation is numerically more efficient than the differential equation formulation as the former solves a surface problem instead of a volume problem. The integral equation formulation is usually solved using the method of moments (MoM). In the MoM, the integral equation formulation is transformed into a matrix formulation, in which the unknown currents are discretized.

The integral equation solved by the MoM can be formulated either in the spectral or in the spatial domain. The difference between these two classes is in the filling of the coupling matrix. In the spectral domain, the moments of the coupling coefficients, i.e., the matrix elements, are in the form of infinite integrals over the spectral variable. Several spectral domain approaches have been applied in the literature on planar guiding structures [5], [6]. In the spatial domain, the elements of the coupling matrix are expressed as finite integrals over the geometrical spatial variables, which can be evaluated efficiently. On the other hand, the evaluation of the Green's functions in the spatial domain results in infinite integrals of the Sommerfeld type. The discrete complex image method (DCIM) can be used in order to accelerate the evaluation of this integral [7]. Several spatial domain MoM have been applied in the literature on multiconductor [8]–[13] and on multislot [7] guiding structures.

All the formulations presented in the literature, as far as we know, treated either a multiconductor or a multislot planar guiding structure. In this paper, a generalized full-wave approach is presented which is capable of analyzing planar guiding structures consisting of both multiconductor and multislot. The approach is based on the integral equation formulation

Manuscript received April 8, 2002; revised October 12, 2002.

E. A. Soliman was with the Interuniversity Microelectronics Centre, B-3001 Leuven, Belgium and also with the Katholieke Universiteit Leuven, B-3001 Leuven, Belgium. He is now with the Department of Electircal and Computer Engineering, McMaster University, Hamilton, ON, Canada L8S 4K1 and also with the Department of Engineering Physics, Cairo University, Cairo, Egypt.

G. A. E. Vandenbosch is with the Telecommunications and Microwaves Section, Katholieke Universiteit Leuven, B-3001 Leuven, Belgium.

E. Beyne is with the High Density Integration and Packaging Group, Interuniversity Microelectronics Centre, B-3001 Leuven, Belgium.

R. P. Mertens is with the Interuniversity Microelectronics Centre, B-3001 Leuven, Belgium and also with the Katholieke Universiteit Leuven, B-3001 Leuven, Belgium.

Digital Object Identifier 10.1109/TMTT.2003.808624

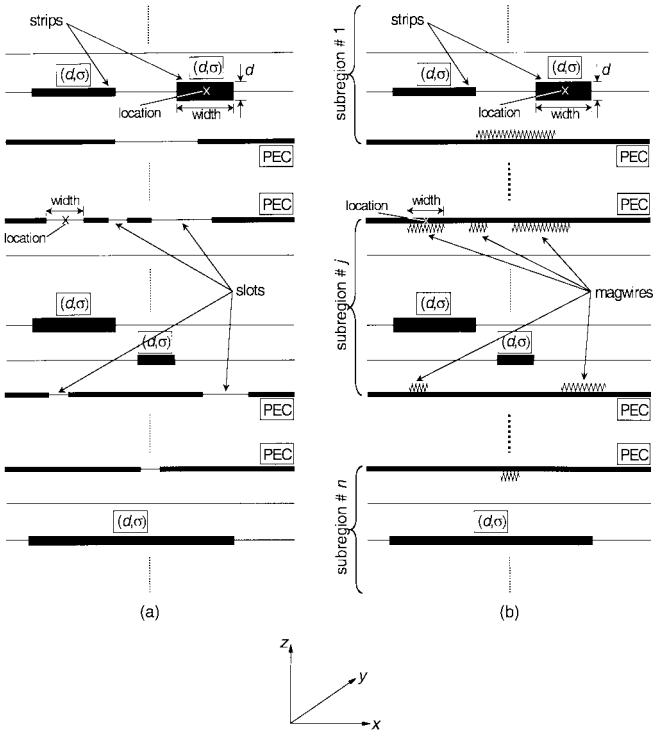

Fig. 1. Planar guiding structure. (a) Original problem. (b) Equivalent problems.

solved by the MoM in the spatial domain. In Section II, the problem under investigation is stated and the notations used are introduced. In Section III, the solution of the individual subregions is presented. An efficient recursive technique for linking the subregion solutions is presented in Section IV. The procedures for evaluating the modal current distribution is presented in Section V. The modal power together with the modal characteristic impedance are evaluated in Section VI. The presented theory is validated by studying number of planar guiding structures in Section VII.

II. Problem Statement

A general planar guiding structure is shown in Fig. 1(a). It consists of an arbitrary number of strips and slots embedded in a stack of dielectric layers. This guiding structure is capable of supporting a number of fundamental modes equal to the total number of strips and slots excluding the infinite perfect electric conductor (PEC) planes, if any. The dielectric layers are assumed to extend infinitely in the lateral plane which lies normal to the direction of stratification. Each strip is characterized by its central location, width, thickness, and conductivity. The slots are carried by PEC planes which, as the abbreviation implies, are assumed to have infinite conductivity. Consequently, the PEC acts as a perfect conducting shielding plane whose thickness is insignificant. Each slot is characterized by its central location and width.

The first step in the solution is to apply the electromagnetic equivalence principle which allows the reduction of the slots in the PEC planes. The electric field of each slot is represented by equivalent magnetic currents located on both sides of the PEC with the same width as the reduced slot. The magnetic currents are infinitely extending along the propagation direction, and they will be referred to as *magwires*, see Fig. 1(b).

The original problem of Fig. 1(a) has been transformed to a number of equivalent problems, subregions, each of which consists of a number of strips and magwires embedded in a reduced set of dielectric layers, as shown in Fig. 1(b). Each subregion is solved separately in Section III. The subregion solutions are linked together in Section IV via the application of the proposed recursive technique. The objective is to evaluate, for each mode, the propagation constant, the dispersion curve, the modal longitudinal and transversal electric and magnetic current, the modal power, and the modal characteristic impedance.

III. Solving Subregions

A. Matrix Formulation

Following the integral equation formulation, the fields can be expressed in terms of the Green's functions and the currents on the strips and magwires through a convolution integral

$$\underline{E}^{e}_{i\ell,\,j}(x) = \int_{x'} G^{e,\,ek}_{ij}\left(|x-x'|\right)\underline{K}^{e}_{j}(x')\,dx' + \underline{\nabla}_{\ell}\int_{x'} G^{e,\,eq}_{ij}\left(|x-x'|\right)\left[\underline{\nabla}'_{\ell}\cdot\underline{K}^{e}_{j}(x')\right]dx' \tag{1}$$

$$\underline{E}^{m}_{i\ell,\,j}(x) = \int_{x'} G^{e,\,mk}_{ij}\left(|x-x'|\right)\left[\underline{u}_{z}\times\underline{K}^{m}_{j}(x')\right]dx' + \underline{\nabla}_{\ell}\int_{x'} G^{e,\,mq}_{ij}\left(|x-x'|\right)\left(\underline{\nabla}'_{\ell}\cdot\left[\underline{u}_{z}\times\underline{K}^{m}_{j}(x')\right]\right)dx' \tag{2}$$

$$\underline{H}^{e}_{i\ell,\,j}(x) = \int_{x'} G^{h,\,ek}_{ij}\left(|x-x'|\right)\left[\underline{u}_{z}\times\underline{K}^{e}_{j}(x')\right]dx' + \underline{\nabla}_{\ell}\int_{x'} G^{h,\,eq}_{ij}\left(|x-x'|\right)\left(\underline{\nabla}'_{\ell}\cdot\left[\underline{u}_{z}\times\underline{K}^{e}_{j}(x')\right]\right)dx' \tag{3}$$

$$\underline{H}^{m}_{i\ell,\,j}(x) = \int_{x'} G^{h,\,mk}_{ij}\left(|x-x'|\right)\underline{K}^{m}_{j}(x')\,dx' + \underline{\nabla}_{\ell}\int_{x'} G^{h,\,mq}_{ij}\left(|x-x'|\right)\left[\underline{\nabla}'_{\ell}\cdot\underline{K}^{m}_{j}(x')\right]dx' \tag{4}$$

where, for the fields on the left-hand sides, the first letter in the subscript indicates the order of the observation interface. The second letter, ℓ, indicates a lateral field component. The third letter in the subscript is the order of the interface carrying the source. The superscript indicates the type of the source: e for electric current and m for magnetic current. The operators $\underline{\nabla}_{\ell} = \partial/\partial x\,\underline{u}_{x} - j\eta\underline{u}_{y}$ and $\underline{\nabla}'_{\ell} = \partial/\partial x'\,\underline{u}_{x} - j\eta\underline{u}_{y}$ refer to the lateral part of the nabla operator in the observation and the source domains, respectively. The derivative with respect to y, $\partial/\partial y$, is replaced by $-j\eta$, because it is assumed that the y-dependence of all fields takes the form $e^{-j\eta y}$, where η is the unknown propagation constant to be determined iteratively. G is

the spatial domain Green's function whose spectral part can be calculated using the technique presented in [14]. The superscript of any Green's function consists of three letters. The first letter indicates the type of the field to be observed, e stands for electric field, while h stands for magnetic field. The second and third letters are related to the source. The second letter indicates the type of the current, e for electric and m for magnetic. The third letter is set to k if the current source is directly used, while it is set to q if the charge derived from the current source is used. K_j^e or K_j^m are the electric or magnetic current on the jth interface, respectively.

The next step is to expand the unknown electric and magnetic currents in terms of known basis functions weighted by unknown expansion coefficients. The longitudinal current is expanded using rectangular functions (Π), while triangular basis functions (Λ) are used to expand the transversal current

$$\Lambda(x) = \begin{cases} (x+\tau)/\tau^2, & -\tau < x < 0 \\ (\tau - x)/\tau^2, & 0 < x < \tau \\ 0, & \text{otherwise} \end{cases} \tag{5}$$

$$\Pi(x) = \begin{cases} 1/\tau, & |x| < \tau/2 \\ 0, & \text{otherwise} \end{cases} \tag{6}$$

where τ is the half-span and the full-span of the triangular and the rectangular basis functions, respectively. Using these basis functions, the current expansion can be written, and then, by applying an appropriate testing procedure, (1)–(4) can be written in a matrix form as follows:

$$\begin{bmatrix} \underbrace{\left[E^{\overleftarrow{\mathrm{L}_1}} K^e\right]}_{N^e \times N^e} & \underbrace{\left[E^{\overleftarrow{\mathrm{L}_1}} K^{m,T}\right]}_{N^e \times N^{m,T}} & \underbrace{\left[E^{\overleftarrow{\mathrm{L}_1}} K^{m,B}\right]}_{N^e \times N^{m,B}} \\ \underbrace{\left[H^T{}^{\overleftarrow{\mathrm{L}_1}} K^e\right]}_{N^{m,T} \times N^e} & \underbrace{\left[H^T{}^{\overleftarrow{\mathrm{L}_1}} K^{m,T}\right]}_{N^{m,T} \times N^{m,T}} & \underbrace{\left[H^T{}^{\overleftarrow{\mathrm{L}_1}} K^{m,B}\right]}_{N^{m,T} \times N^{m,B}} \\ \underbrace{\left[H^B{}^{\overleftarrow{\mathrm{L}_1}} K^e\right]}_{N^{m,B} \times N^e} & \underbrace{\left[H^B{}^{\overleftarrow{\mathrm{L}_1}} K^{m,T}\right]}_{N^{m,B} \times N^{m,T}} & \underbrace{\left[H^B{}^{\overleftarrow{\mathrm{L}_1}} K^{m,B}\right]}_{N^{m,B} \times N^{m,B}} \end{bmatrix} \cdot \begin{bmatrix} \underbrace{[W^e]}_{N^e \times 1} \\ \underbrace{[W^{m,T}]}_{N^{m,T} \times 1} \\ \underbrace{[W^{m,B}]}_{N^{m,B} \times 1} \end{bmatrix} = \begin{bmatrix} \underbrace{[E]}_{N^e \times 1} \\ \underbrace{[H^T]}_{N^{m,T} \times 1} \\ \underbrace{[H^B]}_{N^{m,B} \times 1} \end{bmatrix} \tag{7}$$

where the superscripts T and B mean magnetic current or magnetic field located or observed at the top shielding layer and the bottom shielding layer, respectively. N^e, $N^{m,T}$, and $N^{m,B}$ are the total (both x- and y-directed) number of basis functions representing the electric current, magnetic current on the top shielding layer, and magnetic current on the bottom shielding layer, respectively. The quantities under the braces are the dimensions of the submatrices. The subvectors $[W^e]$, $[W^{m,T}]$, and $[W^{m,B}]$ are the unknown expansion coefficients of the basis functions for the electric current, magnetic current on the top shielding layer, and magnetic current on the bottom shielding layer, respectively. The subvectors $[E]$, $[H^T]$, and $[H^B]$ are the tested tangential electric field on the strips, tangential magnetic field on the top magwires, and tangential magnetic field on the bottom magwires, respectively. The coupling matrices on the left-hand side of (7) are referred to as the *first level coupling matrices* and are denoted by $\overleftarrow{\mathrm{L}_1}$. The elements of these matrices are given in Appendix I.

B. Strips Reduction

Imposing the impedance boundary conditions on the strips, the first row of (7) can be rewritten as follows:

$$\begin{aligned} &\left[E_x{}^{\overleftarrow{\mathrm{L}_1}} K_x^e\right][W_x^e] + \left[E_x{}^{\overleftarrow{\mathrm{L}_1}} K_y^e\right][W_y^e] \\ &\quad + \left[E_x \overleftarrow{\mathrm{L}_1} K^{m,T}\right][W^{m,T}] + \left[E_x \overleftarrow{\mathrm{L}_1} K^{m,B}\right][W^{m,B}] \\ &= [E_x] \end{aligned} \tag{8}$$

$$\begin{aligned} &\left[E_y{}^{\overleftarrow{\mathrm{L}_1}} K_x^e\right][W_x^e] + \left[E_y{}^{\overleftarrow{\mathrm{L}_1}} K_y^e\right][W_y^e] \\ &\quad + \left[E_y \overleftarrow{\mathrm{L}_1} K^{m,T}\right][W^{m,T}] + \left[E_y \overleftarrow{\mathrm{L}_1} K^{m,B}\right][W^{m,B}] \\ &= [E_y] \end{aligned} \tag{9}$$

where the tth element of the vector $[E_x]$ in (8) can be written as follows:

$$E_{x,t} = Z_{s,t}^{\mathrm{eq}} \langle T(x-x_t),\, K_x^e \rangle = Z_{s,t}^{\mathrm{eq}} \int_{D_t} T(x-x_t) K_x^e(x)\, dx \tag{10}$$

where $T(x-x_t)$ is the test function centered around x_t, $K_x^e(x)$ is the x-directed electric current which has been expanded as $\sum_{b=1}^{N_x^e} W_{x,b}^e\, \Lambda(x-x_b)$. $Z_{s,t}^{\mathrm{eq}}$ is the equivalent surface impedance on the strip carrying the tth test function

$$Z_{s,t}^{\mathrm{eq}} = \frac{(1+j)}{2} \sqrt{\frac{\pi f \mu_t}{\sigma_t}}\, \frac{1 + e^{-(1+j)\, d_t \sqrt{\pi f \mu_t \sigma_t}}}{1 - e^{-(1+j)\, d_t \sqrt{\pi f \mu_t \sigma_t}}} \tag{11}$$

where μ_t, σ_t, and d_t are the permeability, conductivity, and thickness of the conductor carrying the tth test function, respectively. The expression given in (11) is derived in Appendix II. It can efficiently account for the thickness and finite conductivity of the conductor as long as its thickness is much smaller than its width. This assumption is satisfied for most practical situations. It has been demonstrated in [15] that, for the selected types of basis functions, the optimum choice of the test function T is the rectangular function Π. Consequently, three basis functions are overlapping with the domain of the test function $\Pi(x-x_t)$, namely $\Lambda(x-x_{t-1})$, $\Lambda(x-x_t)$, and $\Lambda(x-x_{t+1})$ [see Fig. 2(a)].

Performing the inner product in (10), after simple manipulation, one can write

$$E_{x,t} = Z_{s,t}^{\mathrm{eq}} \left(\frac{1}{8\tau_t} W_{x,t-1}^e + \frac{3}{4\tau_t} W_{x,t}^e + \frac{1}{8\tau_t} W_{x,t+1}^e \right) \tag{12}$$

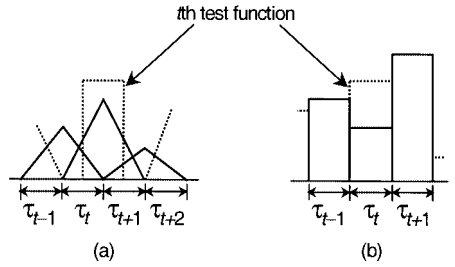

Fig. 2. Basis functions overlapping with the domain of a test function: (a) transversal and (b) longitudinal current.

where τ_t is the full-span and the half-span of the rectangular test function and the triangular basis function, respectively, centered around x_t. It is assumed in writing (12) that the adjacent basis functions have the same span. However, basis functions located on different strips can have different spans. Substituting (12) into (8), one can write

$$\left[E_x \overleftarrow{\mathrm{L}_1'} K_x^e\right][W_x^e] + \left[E_x \overleftarrow{\mathrm{L}_1} K_y^e\right][W_y^e] + \left[E_x \overleftarrow{\mathrm{L}_1} K^{m,T}\right][W^{m,T}] + \left[E_x \overleftarrow{\mathrm{L}_1} K^{m,B}\right][W^{m,B}] = [0] \quad (13)$$

where the matrix $[E_x \overleftarrow{\mathrm{L}_1'} K_x^e]$ is the *modified coupling matrix at the first level*, which takes the form shown in (14) at the bottom of this page.

Similarly, the same analysis is performed on (9), taking into account that in testing the y-directed electric current the tth test function is overlapping with the tth basis function only, as shown in Fig. 2(b). The manipulation yields the following equations:

$$\left[E_y \overleftarrow{\mathrm{L}_1} K_x^e\right][W_x^e] + \left[E_y \overleftarrow{\mathrm{L}_1'} K_y^e\right][W_y^e] + \left[E_y \overleftarrow{\mathrm{L}_1'} K^{m,T}\right][W^{m,T}] + \left[E_y \overleftarrow{\mathrm{L}_1} K^{m,B}\right][W^{m,B}] = [0] \quad (15)$$

$$\left[E_y \overleftarrow{\mathrm{L}_1'} K_y^e\right] = \left[E_y \overleftarrow{\mathrm{L}_1'} K_y^e\right] - \begin{bmatrix} \frac{Z_{s,1}^{\mathrm{eq}}}{\tau_1} & 0 & \cdots & 0 & 0 \\ 0 & \frac{Z_{s,2}^{\mathrm{eq}}}{\tau_2} & \cdots & 0 & 0 \\ \vdots & \vdots & \ddots & \vdots & \vdots \\ 0 & 0 & \cdots & \frac{Z_{s,N_y-1}^{\mathrm{eq}}}{\tau_{N_y-1}} & 0 \\ 0 & 0 & \cdots & 0 & \frac{Z_{s,N_y}^{\mathrm{eq}}}{\tau_{N_y}} \end{bmatrix}. \quad (16)$$

Substituting (13) and (15) into (8) and (9), and combining the resulting equations, one can write

$$\left[E \overleftarrow{\mathrm{L}_1'} K^e\right][W^e] + \left[E \overleftarrow{\mathrm{L}_1} K^{m,T}\right][W^{m,T}] + \left[E \overleftarrow{\mathrm{L}_1} K^{m,B}\right][W^{m,B}] = [0] \quad (17)$$

where the matrix $[E \overleftarrow{\mathrm{L}_1'} K^e]$ is a modified version from the matrix $[E \overleftarrow{\mathrm{L}_1} K^e]$, where the diagonal submatrices of the former can be expressed in terms of the diagonal submatrices of the latter as stated in (14) and (16). It is worth noting that, for the special case of a perfectly conducting strip with zero thickness, the boundary condition requires the tangential electric field to vanish on the strip. Consequently, the matrix $[E \overleftarrow{\mathrm{L}_1'} K^e]$ is identical to the matrix $[E \overleftarrow{\mathrm{L}_1} K^e]$ for this special case.

Using (17), the electric current on the strips can be expressed in terms of the magnetic current on the magwires in both shielding layers

$$[W^e] = -\left[E \overleftarrow{\mathrm{L}_1'} K^e\right]^{-1}\left[E \overleftarrow{\mathrm{L}_1} K^{m,T}\right][W^{m,T}] - \left[E \overleftarrow{\mathrm{L}_1'} K^e\right]^{-1}\left[E \overleftarrow{\mathrm{L}_1} K^{m,B}\right][W^{m,B}]. \quad (18)$$

$$\left[E_x \overleftarrow{\mathrm{L}_1'} K_x^e\right] = \left[E_x \overleftarrow{\mathrm{L}_1} K_x^e\right] - \begin{bmatrix} \frac{3Z_{s,1}^{\mathrm{eq}}}{4\tau_1} & \frac{Z_{s,1}^{\mathrm{eq}}}{8\tau_1} & 0 & \cdots & 0 & 0 & 0 \\ \frac{Z_{s,2}^{\mathrm{eq}}}{8\tau_2} & \frac{3Z_{s,2}^{\mathrm{eq}}}{4\tau_2} & \frac{Z_{s,2}^{\mathrm{eq}}}{8\tau_2} & \cdots & 0 & 0 & 0 \\ \vdots & \vdots & \vdots & \ddots & \vdots & \vdots & \vdots \\ 0 & 0 & 0 & \cdots & \frac{Z_{s,N_x-1}^{\mathrm{eq}}}{8\tau_{N_x-1}} & \frac{3Z_{s,N_x-1}^{\mathrm{eq}}}{4\tau_{N_x-1}} & \frac{Z_{s,N_x-1}^{\mathrm{eq}}}{8\tau_{N_x-1}} \\ 0 & 0 & 0 & \cdots & 0 & \frac{Z_{s,N_x}^{\mathrm{eq}}}{8\tau_{N_x}} & \frac{3Z_{s,N_x}^{\mathrm{eq}}}{4\tau_{N_x}} \end{bmatrix} \quad (14)$$

Substituting (18) into the second and the third rows of (7), and after some manipulations, the following equation can be written:

$$\begin{bmatrix} \left[H^T \overleftarrow{\mathrm{L}_2} K^{m,T}\right] & \left[H^T \overleftarrow{\mathrm{L}_2} K^{m,B}\right] \\ \left[H^B \overleftarrow{\mathrm{L}_2} K^{m,T}\right] & \left[H^B \overleftarrow{\mathrm{L}_2} K^{m,B}\right] \end{bmatrix} \begin{bmatrix} [W^{m,T}] \\ [W^{m,B}] \end{bmatrix} = \begin{bmatrix} [H^T] \\ [H^B] \end{bmatrix} \quad (19)$$

where the submatrices on the left-hand side of (19) are referred to as the *second level coupling matrices*, which can be expressed in terms of the first level coupling matrices as follows:

$$\left[H^T \overleftarrow{\mathrm{L}_2} K^{m,T}\right] = \left[H^T \overleftarrow{\mathrm{L}_1} K^{m,T}\right] - \left[H^T \overleftarrow{\mathrm{L}_1} K^e\right] \cdot \left[E \overleftarrow{\mathrm{L}_1'} K^e\right]^{-1} \left[E \overleftarrow{\mathrm{L}_1} K^{m,T}\right] \quad (20)$$

$$\left[H^T \overleftarrow{\mathrm{L}_2} K^{m,B}\right] = \left[H^T \overleftarrow{\mathrm{L}_1} K^{m,B}\right] - \left[H^T \overleftarrow{\mathrm{L}_1} K^e\right] \cdot \left[E \overleftarrow{\mathrm{L}_1'} K^e\right]^{-1} \left[E \overleftarrow{\mathrm{L}_1} K^{m,B}\right] \quad (21)$$

$$\left[H^B \overleftarrow{\mathrm{L}_2} K^{m,T}\right] = \left[H^B \overleftarrow{\mathrm{L}_1} K^{m,T}\right] - \left[H^B \overleftarrow{\mathrm{L}_1} K^e\right] \cdot \left[E \overleftarrow{\mathrm{L}_1'} K^e\right]^{-1} \left[E \overleftarrow{\mathrm{L}_1} K^{m,T}\right] \quad (22)$$

$$\left[H^B \overleftarrow{\mathrm{L}_2} K^{m,B}\right] = \left[H^B \overleftarrow{\mathrm{L}_1} K^{m,B}\right] - \left[H^B \overleftarrow{\mathrm{L}_1} K^e\right] \cdot \left[E \overleftarrow{\mathrm{L}_1'} K^e\right]^{-1} \left[E \overleftarrow{\mathrm{L}_1} K^{m,B}\right]. \quad (23)$$

At the end of the subregion solving procedure, the matrix equation representing the subregion is modified from (7) to (19). In (19), the electric current on the strips has disappeared, as a consequence of the application of the boundary conditions on the strips. The magnetic field on the magwires is expressed in terms of the magnetic currents flowing on them, through higher level coupling coefficients which internally take the coupling through the strips into account. The above procedure is applied to all the subregions in the problem, one by one. The remaining boundary conditions to be satisfied are the continuity of the electric field and the magnetic field through the slots, located in the PEC shielding layers. This will be carried out in the next section.

IV. Linking Subregion Solutions

The linking of two subregions means satisfying the boundary conditions on the slots located in the common shielding layer. It is assumed that the strips have been eliminated from all the subregions in the previous step. The linking procedure starts from the top-most subregion toward the bottom-most one in a recursive algorithm. Considering the first, the top-most, and the second subregion, their matrix formulations can be written as follows:

$$\left[H_1^B \overleftarrow{\mathrm{L}_2} K_1^{m,B}\right] \left[W_1^{m,B}\right] = \left[H_1^B\right] \quad (24)$$

$$\begin{bmatrix} \left[H_2^T \overleftarrow{\mathrm{L}_2} K_2^{m,T}\right] & \left[H_2^T \overleftarrow{\mathrm{L}_2} K_2^{m,B}\right] \\ \left[H_2^B \overleftarrow{\mathrm{L}_2} K_2^{m,T}\right] & \left[H_2^B \overleftarrow{\mathrm{L}_2} K_2^{m,B}\right] \end{bmatrix} \begin{bmatrix} \left[W_2^{m,T}\right] \\ \left[W_2^{m,B}\right] \end{bmatrix} = \begin{bmatrix} \left[H_2^T\right] \\ \left[H_2^B\right] \end{bmatrix} \quad (25)$$

where the subscripts 1 and 2 are used for the matrix formulation of the first and second subregions, respectively. The continuity of the tangential electric field along the common slots requires that the magnetic current flowing along the magwires at both sides of the common shielding layer are equal in magnitude and opposite in direction. Mathematically, this statement can be written as follows:

$$\left[W_1^{m,B}\right] = -\left[W_2^{m,T}\right]. \quad (26)$$

The remaining boundary condition to be satisfied is the continuity of the tangential magnetic field

$$\left[H_1^B\right] = \left[H_2^T\right]. \quad (27)$$

Using (26) and (27) in (24) and (25) yields

$$\left[W_1^{m,B}\right] = -\left[W_2^{m,T}\right] = \left[\left[H_1^B \overleftarrow{\mathrm{L}_2} K_1^{m,B}\right] + \left[H_2^T \overleftarrow{\mathrm{L}_2} K_2^{m,T}\right]\right]^{-1} \cdot \left[H_2^T \overleftarrow{\mathrm{L}_2} K_2^{m,B}\right] \left[W_2^{m,B}\right]. \quad (28)$$

Substituting (28) into the bottom row of (25), after simple manipulation, yields

$$\left[H_2^B \overleftarrow{\mathrm{L}_3} K_2^{m,B}\right] \left[W_2^{m,B}\right] = \left[H_2^B\right] \quad (29)$$

where $[H_2^B \overleftarrow{\mathrm{L}_3} K_2^{m,B}]$ is referred to as the *third level coupling matrix*, which can be written in terms of the second level coupling matrices as follows:

$$\left[H_2^B \overleftarrow{\mathrm{L}_3} K_2^{m,B}\right] = \left[H_2^B \overleftarrow{\mathrm{L}_2} K_2^{m,B}\right] - \left[H_2^B \overleftarrow{\mathrm{L}_2} K_2^{m,T}\right] \cdot \left[\left[H_1^B \overleftarrow{\mathrm{L}_2} K_1^{m,B}\right] + \left[H_2^T \overleftarrow{\mathrm{L}_2} K_2^{m,T}\right]\right]^{-1} \cdot \left[H_2^T \overleftarrow{\mathrm{L}_2} K_2^{m,B}\right]. \quad (30)$$

Equation (29) can be considered as the matrix formulation of the first and second subregions after linking them together.

It represents the coupling between the magnetic current on the bottom shielding layer of the second subregion and the magnetic field observed on that shielding layer. The third level coupling matrix used in this equation takes into account the presence of magnetic current on the bottom and the top shielding layers of the first and second subregions, respectively. It is expressed in terms of the second level coupling matrices of both subregions [see (30)]. As shown in the previous section, the second level coupling matrices take the coupling through the strips, in their subregions, into account. Consequently, (29) incorporates all coupling mechanisms in both subregions, and solving this equation for $[W_2^{m,B}]$ yields all the remaining unknowns using (28) and (18). Comparing (24) and (29), it is clear that they are identical except for the type of the coupling matrices, second level and third level, respectively. Consequently, the linking procedure explained can be applied in a recursive way starting with the second subregion and ending with the last but one subregion, the $(n-1)$th subregion. The recursive system, for evaluating the third level coupling matrices, can be described in terms of (30) and the general equation relating the jth and the $(j-1)$th matrices as

$$\begin{aligned}\left[H_j^B \overleftarrow{\mathrm{L}_3} K_j^{m,B}\right]\Big|_{j:2\to(n-1)} &= \left[H_j^B \overleftarrow{\mathrm{L}_2} K_j^{m,B}\right] - \left[H_j^B \overleftarrow{\mathrm{L}_2} K_j^{m,T}\right] \\ &\cdot \left[\left[H_{j-1}^B \overleftarrow{\mathrm{L}_3} K_{j-1}^{m,B}\right] + \left[H_j^T \overleftarrow{\mathrm{L}_2} K_j^{m,T}\right]\right]^{-1} \\ &\cdot \left[H_j^T \overleftarrow{\mathrm{L}_2} K_j^{m,B}\right]. \end{aligned} \tag{31}$$

It is instructive to write down the magnetic current in the top and bottom shielding layers of the jth and the $(j-1)$th subregions, respectively, in terms of the magnetic current on the bottom shielding layer of the jth subregion

$$\begin{aligned}\left[W_{j-1}^{m,B}\right] &= -\left[W_j^{m,T}\right] \\ &= \left[\left[H_{j-1}^B \overleftarrow{\mathrm{L}_3} K_{j-1}^{m,B}\right] + \left[H_j^T \overleftarrow{\mathrm{L}_2} K_j^{m,T}\right]\right]^{-1} \\ &\cdot \left[H_j^T \overleftarrow{\mathrm{L}_2} K_j^{m,B}\right]\left[W_j^{m,B}\right]. \end{aligned} \tag{32}$$

The final step is to link the bottom-most subregion, the nth, with the $(n-1)$th subregion. The latter subregion has been constructed by linking all the subregions above the bottom-most one. The matrix formulations representing both subregions can be written as follows:

$$\left[H_{n-1}^B \overleftarrow{\mathrm{L}_3} K_{n-1}^{m,B}\right]\left[W_{n-1}^{m,B}\right] = \left[H_{n-1}^B\right] \tag{33}$$

$$\left[H_n^T \overleftarrow{\mathrm{L}_2} K_n^{m,T}\right]\left[W_n^{m,T}\right] = \left[H_n^T\right]. \tag{34}$$

The continuity of the tangential electric and magnetic fields requires that: $[W_{n-1}^{m,B}] = -[W_n^{m,T}]$ and $[H_{n-1}^B] = [H_n^T]$, respectively. Substituting these boundary conditions into (33) and (34) results in

$$\left[\left[H_{n-1}^B \overleftarrow{\mathrm{L}_3} K_{n-1}^{m,B}\right] + \left[H_n^T \overleftarrow{\mathrm{L}_2} K_n^{m,T}\right]\right]\left[W_n^{m,T}\right] = [0]. \tag{35}$$

Equation (35) carries all the physics of the problem as the mutual coupling in all subregions, including coupling through strips and magwires, are incorporated in this equation. The entire problem with all its subregions, strips, and slots is shrinked into an equation involving the slots of the bottom-most subregion. In order to obtain a nontrivial solution of this equation, the determinant of the matrix on the left-hand side should vanish:

$$\left|\left[H_{n-1}^B \overleftarrow{\mathrm{L}_3} K_{n-1}^{m,B}\right] + \left[H_n^T \overleftarrow{\mathrm{L}_2} K_n^{m,T}\right]\right| = f(\eta) = 0. \tag{36}$$

This equation is referred to as the *characteristic equation*, the value of the determinant on the left-hand side depends on the propagation constant in the longitudinal direction, η. This equation is solved iteratively, using Muller's method [16], for the unknown propagation constant η. A large number of roots can be found for the characteristic equation. Among them are the propagation constants of the fundamental modes of the planar guiding structure. The rest correspond to the higher order modes. The whole iterative procedure can be summarized in the flowchart of Fig. 3.

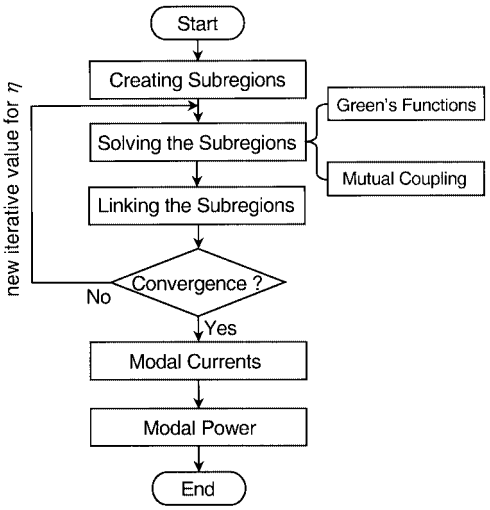

Fig. 3. Flowchart of the major steps of the solution procedure.

V. Modal Current Distribution

Unlike the strips reduction and the linking procedures, the problem is going to be expanded again during the evaluation of the modal currents. After obtaining the propagation constants, (35) can be solved for the magnetic current in the top shielding layer of the bottom-most subregion. Applying a 180° phase shift, the magnetic current on the opposite side of the shielding layer, in the $(n-1)$th subregion, can be obtained. Using (32), the magnetic current on the top shielding layer of the $(n-1)$th subregion can be obtained using the already calculated magnetic current on its bottom shielding layer. This procedure is executed recursively, using (32), starting from the $(n-1)$th subregion

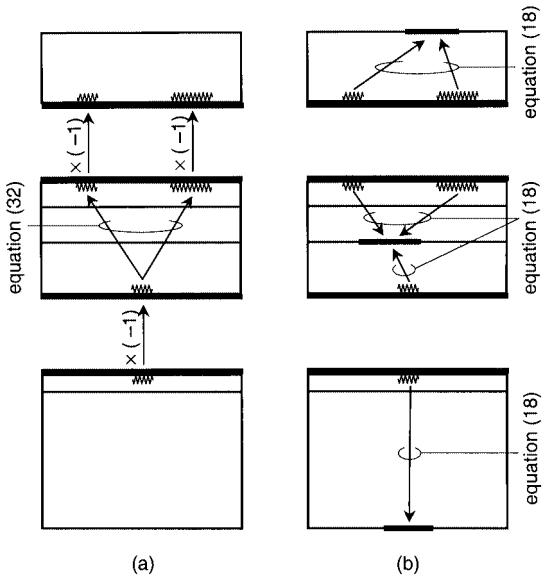

Fig. 4. Evaluation of the modal current distribution. (a) Magnetic current. (b) Electric current.

until the first subregion. Consider, for example, a planar guiding structure like that shown in Fig. 4. The procedure of evaluating the modal magnetic current distribution in all subregions is illustrated in Fig. 4(a).

After evaluating the magnetic currents, each subregion is treated individually in order to evaluate the electric currents on its strips. For this purpose, (18) is used, which expresses the electric current in terms of the magnetic currents on both the top and the bottom shielding layers of a subregion. The procedure for evaluating the electric currents, for the same example, is illustrated in Fig. 4(b).

VI. Modal Power and Modal Characteristic Impedance

The power penetrating the cross section of a general planar guiding structure can be written as follows:

$$P = \mathrm{Re} \sum_s \sum_i \sum_b \int_{-\infty}^{\infty} \int_{z_i}^{z_{i-1}} \left(\underline{E}_{s,i,b} \times \underline{H}^*_{s,i,b} \right) \cdot \underline{u}_y \, dz \, dx \tag{37}$$

where "Re" means "the real part of," and will be suppressed throughout. The summation is carried out over all subregions (s), all layers belonging to the subregion (i), and all basis functions of both electric and magnetic type located inside the subregion (b) (see Fig. 5). z_i and z_{i-1} are the coordinates of the lower and the upper interfaces, respectively, bounding the corresponding layer. $\underline{E}_{s,i,b}$ and $\underline{H}_{s,i,b}$ are the electric and the magnetic field, respectively, in the ith layer of the sth subregion due to the bth basis function. In order to perform the integration over the z axis analytically, Parseval's theorem is used to transform (37) to the spectral domain

$$P = \frac{1}{2\pi} \sum_s \sum_i \sum_b \int_{-\infty}^{\infty} \int_{z_i}^{z_{i-1}} \left(\underline{e}_{s,i,b} \times \underline{h}^*_{s,i,b} \right) \cdot \underline{u}_y \, dz \, d\xi \tag{38}$$

where lower case letters represent spectral domain quantities, ξ is the spectral counterpart of the spatial variable x. The electric

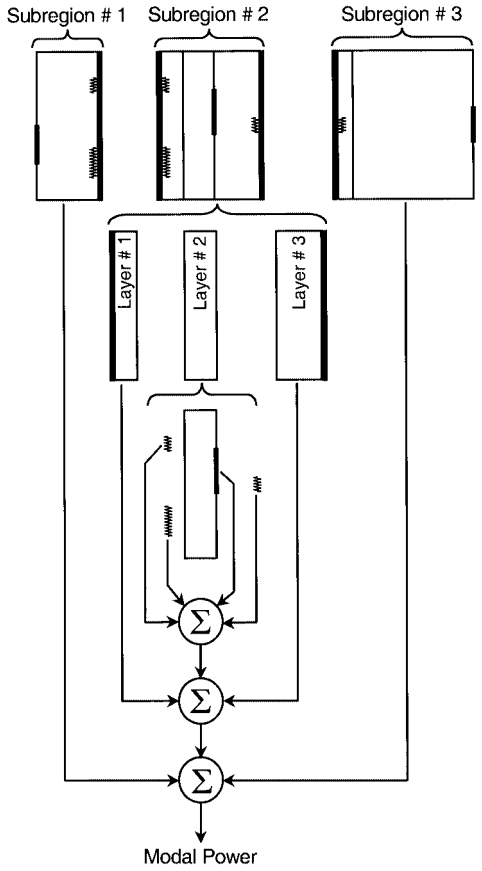

Fig. 5. Evaluation of the modal power.

and the magnetic fields of a basis function can be written in terms of the fields of a unit filamentary source located at the same interface as the basis function as follows:

$$\underline{e}_{s,i,b} = f_b \, \underline{e}^{\,f}_{s,i,b} \tag{39}$$

$$\underline{h}_{s,i,b} = f_b \, \underline{h}^{\,f}_{s,i,b} \tag{40}$$

where $\underline{e}^{\,f}_{s,i,b}$ and $\underline{h}^{\,f}_{s,i,b}$ are the electric and the magnetic field, in the ith layer located within the sth subregion, of a *unit* filamentary source of the same type and located in the same interface as the corresponding bth basis function. If evaluated at the interfaces, these quantities are essentially the spectral domain Green's functions. f_b is the basis function in the spectral domain, which can be obtained by applying the Fourier transform operator on (5) and (6), to yield

$$\tilde{\Lambda}(\xi) = \frac{\sin^2(\tau\xi/2)}{(\tau\xi/2)^2} \tag{41}$$

$$\tilde{\Pi}(\xi) = \frac{\sin(\tau\xi/2)}{(\tau\xi/2)} \tag{42}$$

where $\tilde{\Lambda}$ and $\tilde{\Pi}$ are the spectral counterparts of the spatial basis functions Λ and Π, respectively. The use of small letters for representing the spectral functions is avoided here in order not to confuse with λ and π which have other meanings. Equations (41) and (42) represent the spectral counterpart of spatial basis functions centered at the origin. In general, the spectral domain

equivalent of a spatial function centered around x_b can be obtained by multiplying (41) and (42) by $e^{j\xi x_b}$. Substituting (39) and (40) into (38) and rewriting it in a more compact form yields

$$P = \frac{1}{2\pi} \sum_s \sum_i P_{s,i} \tag{43}$$

where $P_{s,i}$ is the modal power flowing through the cross section of the ith layer which is located in the sth subregion. It can be written as follows:

$$P_{s,i} = \sum_b \int_{-\infty}^{\infty} f_b^2 \int_{z_i}^{z_{i-1}} \left(\underline{e}^{f}_{s,i,b} \times \underline{h}^{f^*}_{s,i,b} \right) \cdot \underline{u}_y \, dz \, d\xi. \tag{44}$$

Decomposing the electromagnetic fields into TE and TM components [14] and omitting the subscripts s and the superscript f from the field quantities, (44) can be rewritten as follows:

$$P_{s,i} = \sum_b \int_{-\infty}^{\infty} f_b^2 \int_{z_i}^{z_{i-1}} \left(e^{\mathrm{TM}}_{i,b,z} h^{\mathrm{TM}^*}_{i,b,x} + e^{\mathrm{TM}}_{i,b,z} h^{\mathrm{TE}^*}_{i,b,x} - e^{\mathrm{TE}}_{i,b,x} h^{\mathrm{TE}^*}_{i,b,z} - e^{\mathrm{TM}}_{i,b,x} h^{\mathrm{TE}^*}_{i,b,z} \right) \cdot dz \, d\xi. \tag{45}$$

The z-dependencies (in the spectral domain) of all field components of both the TE and the TM system are known analytically. The values of the reflection coefficients Γ_i^{TE} and Γ_i^{TM}, which appear in the field expressions in [14], depend only on whether the basis function is located above or under the ith layer. Hence, the summation over the basis functions can be split into two summations: the first one is over the basis functions located above the ith layer, while the second one is over the basis functions under the ith layer. Consequently, one can write the modal power in the ith layer located in the sth subregion as follows:

$$P_{s,i} = \sum_{b,\,\mathrm{above}} \int_{-\infty}^{\infty} f_b^2 \left(p_a^1 + p_a^2 + p_a^3 + p_a^4 \right) d\xi + \sum_{b,\,\mathrm{under}} \int_{-\infty}^{\infty} f_b^2 \left(p_u^1 + p_u^2 + p_u^3 + p_u^4 \right) d\xi \tag{46}$$

where the subscripts a and u denote a basis function located above and under the ith layer, respectively. The power terms in (46) can be written as follows:

$$p^1_{a(u)} = \omega \epsilon_i \left(\frac{\eta}{\beta^2} \right) \left| e^{+,\mathrm{TM}}_{i,b,z} \right|^2 \cdot \int_{z_i}^{z_{i-1}} \left| e^{-\gamma_i z} - \Gamma^{\mathrm{TM}}_{i,a(u)} e^{\gamma_i z} \right|^2 dz \tag{47}$$

$$p^2_{a(u)} = -j \left(\frac{\xi \gamma_i}{\beta^2} \right) e^{+,\mathrm{TM}}_{i,b,z} h^{+,\mathrm{TE}^*}_{i,b,z} \cdot \int_{z_i}^{z_{i-1}} \left(e^{-\gamma_i z} - \Gamma^{\mathrm{TM}}_{i,a(u)} e^{\gamma_i z} \right) \cdot \left(e^{-\gamma_i z} - \Gamma^{\mathrm{TE}}_{i,a(u)} e^{\gamma_i z} \right)^* dz \tag{48}$$

$$p^3_{a(u)} = \omega \mu_i \left(\frac{\eta}{\beta^2} \right) \left| h^{+,\mathrm{TE}}_{i,b,z} \right|^2 \cdot \int_{z_i}^{z_{i-1}} \left| e^{-\gamma_i z} + \Gamma^{\mathrm{TE}}_{i,a(u)} e^{\gamma_i z} \right|^2 dz \tag{49}$$

$$p^4_{a(u)} = -j \left(\frac{\xi \gamma_i}{\beta^2} \right) e^{+,\mathrm{TM}}_{i,b,z} h^{+,\mathrm{TE}^*}_{i,b,z} \cdot \int_{z_i}^{z_{i-1}} \left(e^{-\gamma_i z} + \Gamma^{\mathrm{TM}}_{i,a(u)} e^{\gamma_i z} \right) \cdot \left(e^{-\gamma_i z} + \Gamma^{\mathrm{TE}}_{i,a(u)} e^{\gamma_i z} \right)^* dz \tag{50}$$

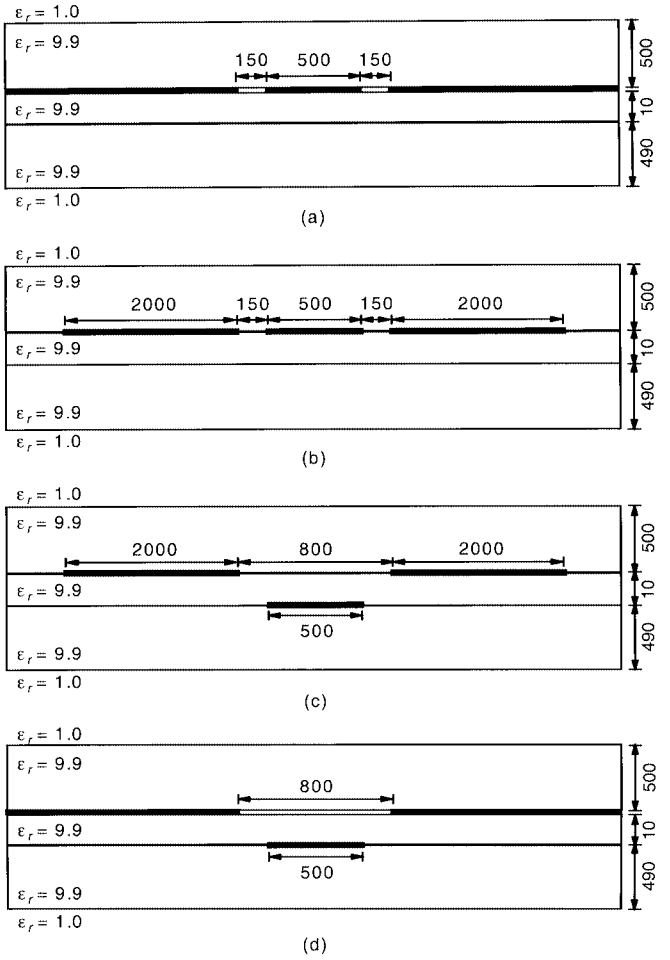

Fig. 6. Canonical structures to the CPW (all dimensions are in μm). (a) CPW line. (b) Finite ground CPW. (c) Dropped central strip finite ground CPW. (d) Dropped central strip CPW.

where $\beta = \sqrt{\xi^2 + \eta^2}$ and $\gamma_i = \sqrt{\beta^2 - \omega^2 \mu_i \varepsilon_i}$. $e^{+,\mathrm{TM}}_{i,b,z}$, $\Gamma^{\mathrm{TM}}_{i,a(u)}$, $h^{+,\mathrm{TE}}_{i,b,z}$, and $\Gamma^{\mathrm{TE}}_{i,a(u)}$ are precalculated spectral domain coefficients [14]. The integrals in (47)–(50) can be evaluated analytically. The remaining integral in (46) along the spectral variable ξ is evaluated numerically. It is worth mentioning that this integral is evaluated a single time for each mode for each frequency point. Consequently, a high degree of computation efficiency is not required for the evaluation of this integral. After evaluating the modal power, the modal characteristic impedance can be obtained as follows:

$$Z_c = P/I^2 = V^2/P \tag{51}$$

where I and V are the modal current and the modal voltage, respectively.

VII. Numerical Results

In this section, the presented theory is applied on a number of planar guiding structures. These structures can be considered as canonical problems to the CPW line. Consequently, comparing the results of these problems with each other and with the CPW provides a self-contained validation procedure. The CPW line together with its canonical structures are shown in Fig. 6. For

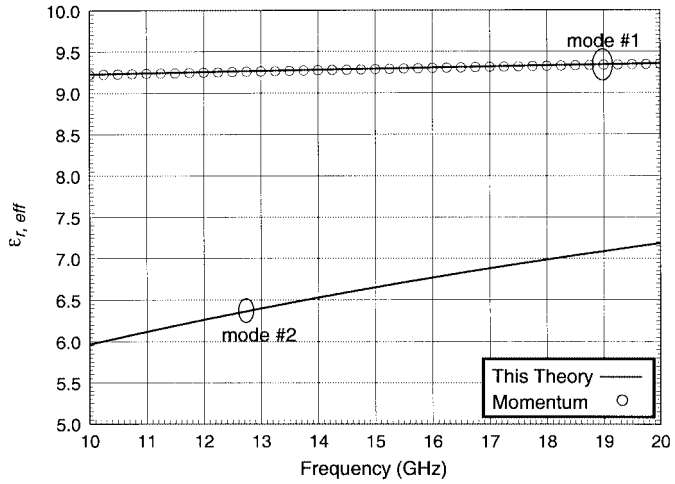

Fig. 7. Effective dielectric constant versus frequency for the CPW line of Fig. 6(a). Three segments are used to represent each slot.

these structures, the conductors are assumed perfect with zero thicknesses.

The effective dielectric constant versus frequency for the conventional CPW of Fig. 6(a) is plotted in Fig. 7 using three segments for representing each slot. The calculations are also performed using HP-Momentum, for comparison, also using three segments of the same width per slot. Perfect agreement is observed for mode #1 (odd). HP-Momentum is not able to provide results for mode #2 (even) of the CPW. The modal current distributions of the CPW are well known and, consequently, they are not presented. The computation time per frequency point for each mode of problem 6(a) using the proposed formulation is 4 s on an HP-9000/782 workstation.

The first canonical problem to the CPW is the finite ground CPW which is formed using three coplanar strips, as shown in Fig. 6(b). The central strip is identical to that of the CPW. The outer strips are sufficiently large to serve as an electrically infinite ground planes. Unlike the CPW line, the triple-stripline has three fundamental modes. The longitudinal and the transversal modal current distributions of the triple-stripline are plotted in Fig. 8(a) and (b), respectively. The outer strips are represented using 20 segments, while five segments are used to represent the central strip. The modal current distributions shown in Fig. 8 are calculated at 15 GHz.

The distribution of the transversal current is 90° leading in phase with respect to that of the longitudinal current distribution. Observing the longitudinal electric current distribution of mode #1 in Fig. 8(a), the currents flowing in the outer strips are identical in phase and magnitude, while they are out-of-phase with the current in the central strip. Consequently, this mode can be considered as analogous to the odd mode of the CPW. For mode #2, the longitudinal currents in the outer strips are equal in magnitude and out-of-phase, while the current flowing in the central strip cancel each other in the integral sense. As a result, we can consider mode #2 as analogous to the even mode of the CPW. The extra mode, #3, of the triple-stripline has all its longitudinal currents in-phase as shown in Fig. 8(a). It is worth mentioning that mode #3 cannot be practically used in transmitting power through the guiding structure as the return path of the

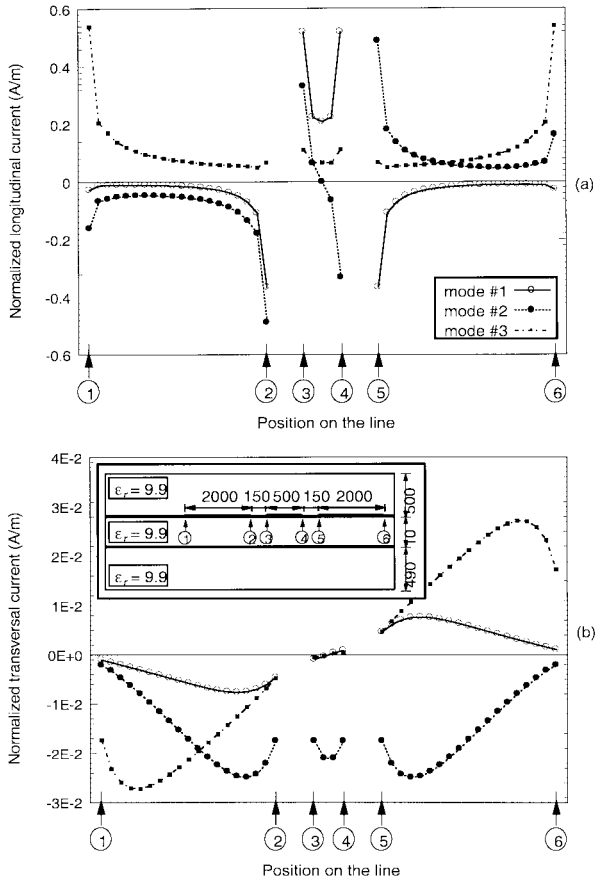

Fig. 8. Normalized modal current distribution of the triple-stripline: (a) longitudinal and (b) transversal. Twenty and five segments are used to represent the outer and the central strips, respectively, $f = 15$ GHz.

current is theoretically located at ∞. Monitoring the transversal current distribution of the three modes in Fig. 8(b), we observe that the phase relations between the currents on the three strips are opposite to the corresponding relations for the longitudinal currents.

The second canonical problem is shown in Fig. 6(c). This structure is formed from the coplanar triple-stripline by dropping the central strip to an intermediate interface laying 10 μm below the interface carrying the outer strips. Physically, this structure should behave almost identical to the coplanar triple-stripline of Fig. 6(b). The modal current distributions of this canonical problem have been evaluated and were found to be identical to the distributions presented in Fig. 8. The computation time per frequency point for each mode of problems 6(b) and (c) using the proposed formulation, is 15 s on an HP-9000/782 workstation.

The last canonical problem of the CPW line is shown in Fig. 6(d). It has been constructed from the CPW line of Fig. 6(a) by dropping the central strip to the same intermediate interface as used in the problem of Fig. 6(c). This structure consists of a single slot in the top subregion and a strip and a slot in the bottom subregion. Consequently, two modes should be considered for this structure. Fig. 9(a) and (b) shows the longitudinal and the transversal modal current distributions, respectively, for the two fundamental modes. The slot has been represented using 25 segments, while 15 segments were used to represent the strip.

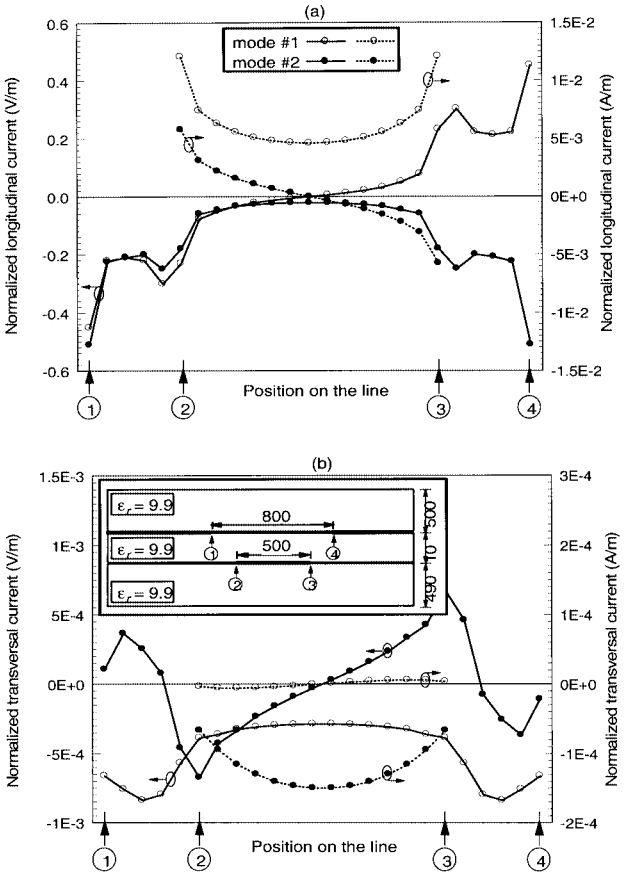

Fig. 9. Normalized modal current distribution of the dropped central strip CPW. (a) Longitudinal. (b) Transversal. Twenty-five and 15 segments are used to represent the slot and the strip, respectively, $f = 15$ GHz.

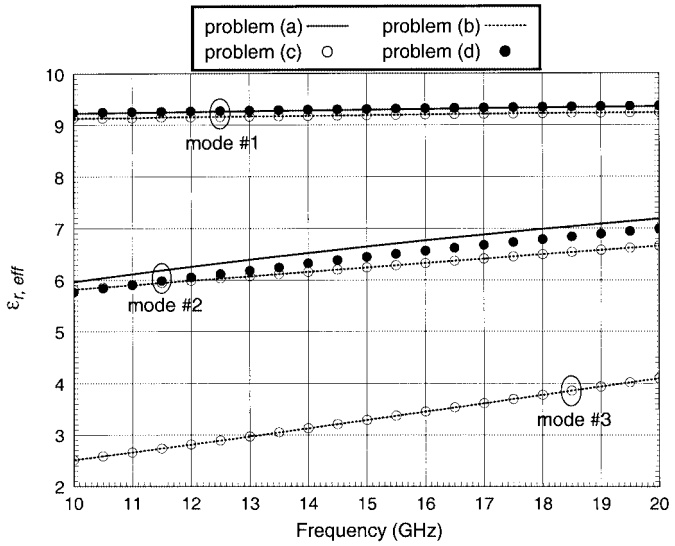

Fig. 10. Effective dielectric constant versus frequency for all the propagating modes of the four canonical problems of Fig. 6.

The modal current calculations are performed at 15 GHz. The transversal current is leading 90° in phase with respect to the longitudinal current. Monitoring the longitudinal current distribution of mode #1, it is clear that the magnetic current distributions near the edges of the slot are equal in magnitude and out-of-phase. Moreover, the electric current distribution on the strip has a significant contribution in the integral sense. Consequently, this mode is analogous to the odd mode of the CPW. Mode #2 has equivalent magnetic currents near the edges of the slot with the same magnitude and phase. In addition, the electric current on the strip has no integral contribution as observed for mode #2 in the previous two canonical problems. Consequently, mode #2 is analogous to the even mode of the CPW line. The computation time per frequency point for each mode of problem Fig. 6(d) using the proposed formulation is 20 s on an HP-9000/782 workstation.

The effective dielectric constant of all the fundamental modes for the four problems of Fig. 6 are plotted versus frequency in Fig. 10. The figure shows that the results for mode #1 are very close to each other in all the four problems. For mode #2, the agreement between the four problems is still good, but not as good as for mode #1. The little deviation for mode #2 can be attributed to the loosely bound nature of the field of the even mode which makes it more sensitive to the truncation of the ground planes. The third mode of problem Fig. 6(b) is in excellent agreement with the third mode of problem Fig. 6(c). Based on the very good agreement between the four canonical problems, the calculated results are validated.

It is worth mentioning here that several other types of planar guiding structures, such as microstrip lines, slotlines, and coupled microstrip lines with different conductors' types and thicknesses and embedded in different layer structures, are studied. The results are, whenever possible, compared with those of HP-Momentum. The comparisons show perfect agreement for both the effective dielectric constant and the characteristic impedance calculations.

VIII. Conclusion

This paper presents a generalized theory for solving planar guiding structure problems. The guiding structure under investigation consists of an arbitrary number of slots and strips of arbitrary widths, thicknesses, and conductivity. The solution is based on the integral equation formulation which has been solved by the MoM. The integral equation is formulated in the spatial domain. All information about the fundamental modes supported by the guiding structure is available. This information includes the modal propagation constant, the longitudinal and the transversal modal electric and magnetic current distribution, the dispersion curves, the modal power, and the modal characteristic impedance.

The presented full-wave techniques in the literature deal with either multiconductor or multislot planar guiding structures. In this paper, both types are brought together in a single frame. In this frame, the original problem is split into subproblems, subregions, due to the presence of several PECs carrying slots. Each subregion is solved separately taking all coupling mechanisms into account. A new numerically efficient recursive technique has been presented for linking the solutions of these subproblems together at the end and to evaluate the modal current distribution of the guiding structure. The proposed theory is applied to number of canonical problems, which cannot be solved using the commercial software. The agreement between the calculated results validates the implementation of the theory.

APPENDIX I
FIRST LEVEL COUPLING MATRICES

Each submatrix on the left-hand side of (7) consists of four submatrices

$$\underbrace{\left[F \overleftarrow{\mathrm{L}_1} K\right]}_{N\times N} = \begin{bmatrix} \underbrace{\left[F_x \overleftarrow{\mathrm{L}_1} K_x\right]}_{N_x\times N_x} & \underbrace{\left[F_x \overleftarrow{\mathrm{L}_1} K_y\right]}_{N_x\times N_y} \\ \underbrace{\left[F_y \overleftarrow{\mathrm{L}_1} K_x\right]}_{N_y\times N_x} & \underbrace{\left[F_y \overleftarrow{\mathrm{L}_1} K_y\right]}_{N_y\times N_y} \end{bmatrix} \tag{52}$$

where K refers to the basis functions of electric or magnetic current directed either in the x or in the y direction. Similarly, F refers to the observation fields, electric or magnetic, polarized in either the x or y direction. Following (52), the elements in the submatrices of the left-hand side of (7) take the following form:

$$\left[E_x \overleftarrow{\mathrm{L}_1} K_x^e\right]_{t,b} = \left\langle \Pi(x-x_t),\, \left[G_{ij}^{e;ek} * \Lambda(x'-x_b)\right]\right\rangle + \left\langle \Pi(x-x_t),\, \frac{d}{dx}\left[G_{ij}^{e;eq} * \Lambda'(x'-x_b)\right]\right\rangle \tag{53}$$

$$\left[E_x \overleftarrow{\mathrm{L}_1} K_y^e\right]_{t,b} = -j\eta\left\langle \Pi(x-x_t),\, \frac{d}{dx}\left[G_{ij}^{e;eq} * \Pi(x'-x_b)\right]\right\rangle \tag{54}$$

$$\left[E_y \overleftarrow{\mathrm{L}_1} K_x^e\right]_{t,b} = -j\eta\left\langle \Pi(x-x_t),\, \left[G_{ij}^{e;eq} * \Lambda'(x'-x_b)\right]\right\rangle \tag{55}$$

$$\left[E_y \overleftarrow{\mathrm{L}_1} K_y^e\right]_{t,b} = \left\langle \Pi(x-x_t),\, \left[G_{ij}^{e;ek} * \Pi(x'-x_b)\right]\right\rangle - \eta^2\left\langle \Pi(x-x_t),\, \left[G_{ij}^{e;eq} * \Pi(x'-x_b)\right]\right\rangle \tag{56}$$

$$\left[E_x \overleftarrow{\mathrm{L}_1} K_x^m\right]_{t,b} = -j\eta\left\langle \Pi(x-x_t),\, \frac{d}{dx}\left[G_{ij}^{e;mq} * \Lambda(x'-x_b)\right]\right\rangle \tag{57}$$

$$\left[E_x \overleftarrow{\mathrm{L}_1} K_y^m\right]_{t,b} = -\left\langle \Pi(x-x_t),\, \left[G_{ij}^{e;mk} * \Pi(x'-x_b)\right]\right\rangle - \left\langle \Pi(x-x_t),\, \frac{d}{dx}\left[G_{ij}^{e;mq} * \Pi'(x'-x_b)\right]\right\rangle \tag{58}$$

$$\left[E_y \overleftarrow{\mathrm{L}_1} K_x^m\right]_{t,b} = \left\langle \Pi(x-x_t),\, \left[G_{ij}^{e;mk} * \Lambda(x'-x_b)\right]\right\rangle - \eta^2\left\langle \Pi(x-x_t),\, \left[G_{ij}^{e;mq} * \Lambda(x'-x_b)\right]\right\rangle \tag{59}$$

$$\left[E_y \overleftarrow{\mathrm{L}_1} K_y^m\right]_{t,b} = j\eta\left\langle \Pi(x-x_t),\, \left[G_{ij}^{e;mq} * \Pi'(x'-x_b)\right]\right\rangle \tag{60}$$

$$\left[H_x \overleftarrow{\mathrm{L}_1} K_x^e\right]_{t,b} = -j\eta\left\langle \Pi(x-x_t),\, \frac{d}{dx}\left[G_{ij}^{h;eq} * \Lambda(x'-x_b)\right]\right\rangle \tag{61}$$

$$\left[H_x \overleftarrow{\mathrm{L}_1} K_y^e\right]_{t,b} = -\left\langle \Pi(x-x_t),\, \left[G_{ij}^{h;ek} * \Pi(x'-x_b)\right]\right\rangle - \left\langle \Pi(x-x_t),\, \frac{d}{dx}\left[G_{ij}^{h;eq} * \Pi'(x'-x_b)\right]\right\rangle \tag{62}$$

$$\left[H_y \overleftarrow{\mathrm{L}_1} K_x^e\right]_{t,b} = \left\langle \Pi(x-x_t),\, \left[G_{ij}^{h;ek} * \Lambda(x'-x_b)\right]\right\rangle - \eta^2\left\langle \Pi(x-x_t),\, \left[G_{ij}^{h;eq} * \Lambda(x'-x_b)\right]\right\rangle \tag{63}$$

$$\left[H_y \overleftarrow{\mathrm{L}_1} K_y^e\right]_{t,b} = j\eta\left\langle \Pi(x-x_t),\, \left[G_{ij}^{h;eq} * \Pi'(x'-x_b)\right]\right\rangle \tag{64}$$

$$\left[H_x \overleftarrow{\mathrm{L}_1} K_x^m\right]_{t,b} = \left\langle \Pi(x-x_t),\, \left[G_{ij}^{h;mk} * \Lambda(x'-x_b)\right]\right\rangle + \left\langle \Pi(x-x_t),\, \frac{d}{dx}\left[G_{ij}^{h;mq} * \Lambda'(x'-x_b)\right]\right\rangle \tag{65}$$

$$\left[H_x \overleftarrow{\mathrm{L}_1} K_y^m\right]_{t,b} = -j\eta\left\langle \Pi(x-x_t),\, \frac{d}{dx}\left[G_{ij}^{h;mq} * \Pi'(x'-x_b)\right]\right\rangle \tag{66}$$

$$\left[H_y \overleftarrow{\mathrm{L}_1} K_x^m\right]_{t,b} = -j\eta\left\langle \Pi(x-x_t),\, \left[G_{ij}^{h;mq} * \Lambda'(x'-x_b)\right]\right\rangle \tag{67}$$

$$\left[H_y \overleftarrow{\mathrm{L}_1} K_y^m\right]_{t,b} = \left\langle \Pi(x-x_t),\, \left[G_{ij}^{h;mk} * \Pi(x'-x_b)\right]\right\rangle - \eta^2\left\langle \Pi(x-x_t),\, \left[G_{ij}^{h;mq} * \Pi(x'-x_b)\right]\right\rangle \tag{68}$$

where the subscripts t and b on the left-hand side are the orders of the test and the basis function, respectively, which correspond to the row and the column order, respectively, in the submatrix. The subscripts i and j of the Green's functions refer to the order of the interface carrying the test and the basis functions, respectively. x_t and x_b are the center coordinates of the test and the basis function, respectively.

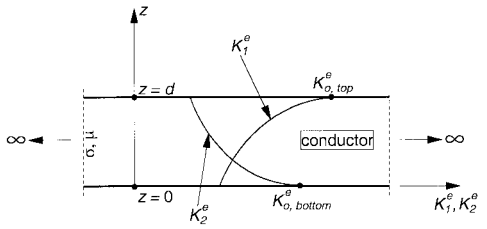

Fig. 11. Cross section of a current carrying conducting layer.

The operation $\langle f_t,\ f\rangle$ means innerproduct, while $[G*f_b]$ means convolution:

$$\langle f_t(x),\ f(x)\rangle = \int_{D_t} f_t(x) f(x)\, dx \tag{69}$$

$$[G*f_b] = \int_{D_b} G(|x-x'|)\, f_b(x')\, dx' \tag{70}$$

where D_t and D_b are the domains of the test and the basis functions, respectively. Λ' and Π' are the derivatives of the basis functions Λ and Π, respectively. The superscripts T and B, indicating top and bottom shielding layers, have been removed from (53)–(68) as the expressions of the coupling coefficients are the same for both of them. In (53)–(68), the razor-blade testing scheme is adopted because it gives more physical modal current distribution near the edges than that obtained using Galerkin testing [15].

APPENDIX II
EQUIVALENT SURFACE IMPEDANCE

In this Appendix, the formula used for the surface impedance in (11) is derived. Fig. 11 shows a conductor layer with thickness d, conductance σ, and permeability μ. The conductor is assumed to extend infinitely in the lateral direction. This assumption is reasonable as long as the conductor width is much larger than its thickness. The current density penetrating the cross section of the conductor can be expanded in terms of its values at the two surfaces as follows (see Fig. 11):

$$\begin{aligned} K^e(z) &= K_1^e(z) + K_2^e(z) \\ &= K_{0,\,\mathrm{top}}^e e^{(1+j)(z-d)/\delta} + K_{0,\,\mathrm{bottom}}^e e^{-(1+j)z/\delta} \end{aligned} \tag{71}$$

where $K_{0,\,\mathrm{top}}^e$ and $K_{0,\,\mathrm{bottom}}^e$ are the electric current density on the top and the bottom surface of the conductor, respectively. z is the axis normal to the conductor layer and δ is the skin depth: $\delta = \sqrt{1/(\pi f \mu \sigma)}$. The longitudinal current can be obtained by integrating the current density in (71) along the conductor thickness

$$\begin{aligned} K_\ell^e &= \int_0^d K^e(z)\, dz \\ &= \frac{\delta}{(1+j)} \left[1 - e^{-(1+j)d/\delta}\right] \left(K_{0,\,\mathrm{top}}^e + K_{0,\,\mathrm{bottom}}^e\right). \end{aligned} \tag{72}$$

Since $K^e(z) = \sigma E(z)$, one can write the following equations at the top and the bottom surfaces of the conductor:

$$\sigma E(d) = K^e(d) = K_{0,\,\mathrm{top}}^e + K_{0,\,\mathrm{bottom}}^e e^{-(1+j)d/\delta} \tag{73}$$

$$\sigma E(0) = K^e(0) = K_{0,\,\mathrm{top}}^e e^{-(1+j)d/\delta} + K_{0,\,\mathrm{bottom}}^e. \tag{74}$$

Summing (73) and (74), we have

$$E(d) + E(0) = \frac{1}{\sigma}\left[1 + e^{-(1+j)d/\delta}\right]\left(K_{0,\,\mathrm{top}}^e + K_{0,\,\mathrm{bottom}}^e\right). \tag{75}$$

Writing the surface impedance boundary condition yields

$$\left[E(d) + E(0)\right]/2 = Z_s^{\mathrm{eq}} K_\ell^e. \tag{76}$$

Comparing (72), (75), and (76) yields the required expression for the equivalent surface impedance

$$Z_s^{\mathrm{eq}} = \frac{(1+j)}{2}\sqrt{\frac{\pi f \mu}{\sigma}}\,\frac{1 + e^{-(1+j)d\sqrt{\pi f \mu \sigma}}}{1 - e^{-(1+j)d\sqrt{\pi f \mu \sigma}}}. \tag{77}$$

REFERENCES

[1] J. Bernal, F. Medina, and M. Horno, "Quick quasi-TEM analysis of multiconductor transmission lines with rectangular cross section," *IEEE Trans. Microwave Theory Tech.*, vol. 45, pp. 1619–1626, Sept. 1997.

[2] G. Plaza, F. Mesa, and M. Horno, "Quick computation of $[C]$, $[L]$, $[G]$, and $[R]$ matrices of multiconductor and multilayered transmission systems," *IEEE Trans. Microwave Theory Tech.*, vol. 43, pp. 1623–1626, July 1995.

[3] X. Zhang, J. Fang, K. K. Mei, and Y. Liu, "Calculation of the dispersive characteristics of microstrips by the time-domain finite-difference method," *IEEE Trans. Microwave Theory Tech.*, vol. 36, pp. 263–267, Feb. 1988.

[4] M. S. Alam, M. Koshiba, K. Hirayama, and Y. Hayashi, "Hybrid-mode analysis of multilayered and multiconductor transmission lines," *IEEE Trans. Microwave Theory Tech.*, vol. 45, pp. 205–211, Feb. 1997.

[5] G. Cano, F. Medina, and M. Horno, "Efficient spectral domain analysis of generalized multistrip lines in stratified media including thin, anisotropic, and lossy substrates," *IEEE Trans. Microwave Theory Tech.*, vol. 40, pp. 217–227, Feb. 1992.

[6] T. Kitazawa, "Nonreciprocity of phase constants, characteristic impedances, and conductor losses in planar transmission lines with layered anisotropic media," *IEEE Trans. Microwave Theory Tech.*, vol. 43, pp. 445–451, Feb. 1995.

[7] E. A. Soliman, P. Pieters, E. Beyne, and G. A. E. Vandenbosch, "Numerically efficient spatial domain moment method for multislot transmission lines in layered media—Application to multislot lines in MCM-D technology," *IEEE Trans. Microwave Theory Tech.*, vol. 47, pp. 1782–1787, Sept. 1999.

[8] N. Fache and D. De Zutter, "Rigorous full-wave space-domain solution for dispersive microstrip lines," *IEEE Trans. Microwave Theory Tech.*, vol. 36, pp. 731–737, Apr. 1988.

[9] J. F. Kiang, "Integral equation solution of the skin effect problem in conductor strips of finite thickness," *IEEE Trans. Microwave Theory Tech.*, vol. 39, pp. 452–460, Mar. 1991.

[10] K. A. Michalski and D. Zheng, "Rigorous analysis of open microstrip lines of arbitrary cross section in bound and leaky regimes," *IEEE Trans. Microwave Theory Tech.*, vol. 37, pp. 2005–2010, Dec. 1989.

[11] N. Fache and D. De Zutter, "Full-wave analysis of a perfectly conducting wire transmission line in a double-layered conductor-backed medium," *IEEE Trans. Microwave Theory Tech.*, vol. 37, pp. 512–518, Mar. 1989.

[12] N. Fache, F. Olyslager, and D. De Zutter, "Full-wave analysis of coupled perfectly conducting wires in a multilayered medium," *IEEE Trans. Microwave Theory Tech.*, vol. 39, pp. 673–680, Apr. 1991.

[13] C.-I. G. Hsu, R. F. Harrington, K. A. Michaliski, and D. Zheng, "Analysis of multiconductor transmission lines of arbitrary cross section in multilayered uniaxial media," *IEEE Trans. Microwave Theory Tech.*, vol. 41, pp. 70–78, Jan. 1993.

[14] G. A. E. Vandenbosch and A. R. Van de Capelle, "Mixed-potential integral expression formulation of the electric field in a stratified dielectric medium—Application to the case of a probe current source," *IEEE Trans. Antennas Propagat.*, vol. 40, pp. 806–817, July 1992.

[15] E. A. Soliman, G. A. E. Vandenbosch, and E. Beyne, "Galerkin versus razor-blade testing in the method of moments formulation for multiconductor transmission lines," *Int. J. RF Microwave Computer-Aided Eng.*, vol. 10, pp. 132–138, Mar. 2000.

[16] S. D. Conte and C. de Boor, *Elementary Numerical Analysis: An Algorithmic Approach*. New York: McGraw-Hill, 1990.

Ezzeldin A. Soliman (S'97–A'99) was born in Cairo, Egypt, on May 18, 1970. He received the B.Sc. degree (distinction with honors) in electronics and communications engineering and M.Sc. degree in engineering physics from Cairo University, Giza, Egypt, in 1992 and 1995, respectively, and the Ph.D. degree (*summa cum laude*) in electrical engineering from the University of Leuven, Leuven, Belgium, in 2000.

From 1992 to 1996, he was a Research and Teaching Assistant with the Department of Engineering Physics, Faculty of Engineering, Cairo University. From 1996 to 2000, he was a Research Assistant at both the Interuniversity Microelectronics Centre (IMEC), Leuven, Belgium, and the Department of Electrical Engineering, University of Leuven. From April 2002 to July 2002, he was a Visiting Assistant Professor with IMEC. He is currently a Post-Doctoral Fellow with the Department of Electrical and Computer Engineering, McMaster University, Hamilton, ON, Canada. He is also an Assistant Professor with the Department of Engineering Physics, Faculty of Engineering, Cairo University. His research interests include the integral-equation formulation of planar structures, numerical techniques in electromagnetics, development and characterization of planar antennas in the multilayer thin-film technology, and the neural network modeling of electromagnetic problems.

Guy A. E. Vandenbosch (M'85) was born in Sint-Niklaas, Belgium, on May 4, 1962. He received the M.S. and Ph.D. degrees in electrical engineering from the Katholieke Universiteit Leuven, Leuven, Belgium, in 1985 and 1991, respectively.

From 1985 to 1991, he was a Research and Teaching Assistant with the Telecommunications and Microwaves Section, Katholieke Universiteit Leuven, where he was involved with the modeling of microstrip antennas with the integral-equation technique. From 1991 to 1993, he was a Post-Doctoral Researcher with the Katholieke Universiteit Leuven. He is currently a Professor at the Katholieke Universiteit Leuven. His research interests are electromagnetic theory, computational electromagnetics, planar antennas and circuits, electromagnetic radiation, electromagnetic compatibility, and bioelectromagnetics. His research has been published in international journals and presented at international conferences.

Dr. Vandenbosch is a member of the Management Committee of the European project COST 284 on "Innovative Antennas for Emerging Terrestrial and Space-based Applications." Within this project, he has led the working group on "Models for Antennas and RF Circuit Components." Since 2001, he has been the President of SITEL, the Belgian Society of Engineers in Telecommunications and Electronics. He also currently holds the position of vice-chairman of the IEEE Benelux Chapter on Antennas and Propagation.

Eric Beyne received the M.S. degree in electrical engineering and Ph.D. degree in applied sciences from the University of Leuven, Leuven, Belgium, in 1983 and 1990, respectively.

From 1983 to 1985, he was a Research Assistant with the Department of Electrical Engineering, University of Leuven. In 1986, he joined the Interuniversity Microelectronics Centre (IMEC), Leuven, Belgium, as he worked toward the Ph.D. degree on the interconnection of high-frequency digital circuits. He is currently the Head of the High Density Integration and Packaging (HDIP) Group, IMEC, where he is responsible for projects on multichip modules (MCMs) and advanced packaging.

Dr. Beyne is a member of the IMAPS-Benelux Committee.

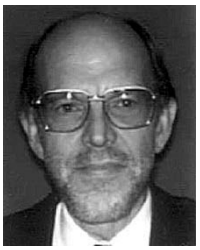

Robert P. Mertens (M'80–SM'86–F'95) received the Ph.D. degree in electrical engineering from the University of Leuven, Leuven, Belgium, in 1972.

In 1973, he was a Visiting Scientist with the University of Florida, Gainesville. Following his return to Belgium in 1974, he became a Senior Research Associate with the National Foundation for Scientific Research of Belgium. In 1984, he joined the Interuniversity Microelectronics Centre (IMEC), Leuven, Belgium, as Vice President, where he is responsible for research on materials and packaging. These activities also include research on microsystems, photovoltaics, and solid-state sensors. Since 1984, he has also been a Professor with the University of Leuven, where he teaches courses on devices and technology of electronic systems.